Extensive mountain glaciation in central Patagonia during Marine Isotope Stage 5

Extensive mountain glaciation in central Patagonia during Marine Isotope Stage 5

Monika Mendelová[a,*], Andrew S. Hein[a], Ángel Rodés[b], Sheng Xu[b]

[a] *University of Edinburgh, School of Geosciences, Drummond Street, Edinburgh, EH8 9XP, Scotland*

[b] *Scottish Universities Environmental Research Centre, Scottish Enterprise Technology Park, East Kilbride, G75 OQF, Glasgow, Scotland*

Abstract

The timing and magnitude of glacial advances throughout a glacial cycle can give insight on the underlying drivers of climate change. Our knowledge of glacial activity early in a glacial cycle, however, is limited by incomplete preservation of the geomorphological record. Here, we present a ^{10}Be-dated glacial chronology from early in the last glacial cycle from the Belgrano valley, east of Monte San Lorenzo in central Patagonia. Our chronology reveals the most extensive glacial advance of the last glacial cycle occurred at $\sim$ 75 ka, at the end of Marine Isotope Stage 5. A second, less-extensive advance occurred at $\sim$ 25 ka during the global Last Glacial Maximum. The topographic setting is such that ice growth would have initiated on and around the San Lorenzo massif at the start of the glacial cycle. We suggest reduced southern hemisphere summer insolation at the time played a significant role in driving this early advance. The comparatively smaller glacier extent during the global Last Glacial Maximum is likely a consequence of the build-up of

*Corresponding author

Email address: m.mendelova@sms.ac.uk (Monika Mendelová)

the full Patagonian Ice Sheet, which would have caused ice-divide migration, ice-flow re-routing, and increased aridity on its lee side.
Keywords: last glacial cycle, cosmogenic nuclide exposure dating, ice-divide migration, South America, glacial chronology

1. Introduction

There is a long standing debate on the timing of glaciation in the southern mid-latitudes, its (a-) synchrony with the northern hemisphere and its forcing mechanisms (Mercer, 1984; Denton et al., 1999a; Sugden et al., 2005). Recent studies in the southern mid-latitudes demonstrated numerous substantial glacial advances, in many cases local maxima, prior to the global Last Glacial Maximum (gLGM, ca. 26 - 19 ka, Clark et al., 2009) (e.g. Zech et al., 2011; Darvill et al., 2015; García et al., 2018; Schaefer et al., 2015; Kelley et al., 2014; Shulmeister et al., 2019; Sutherland et al., 2007). While an early maximum is not uncommon for many mountain glaciers and sectors of large ice sheets (Gillespie and Molnar, 1995; Hughes et al., 2013), it suggests that our understanding of glaciation in the southern mid-latitudes and, in particular its drivers, is incomplete. Orbital parameters, including regional insolation and season duration, latitudinal shifts in southern westerly winds (SWW) and associated oceanic systems, as well as local ice dynamics have been invoked as potential drivers of pre-LGM ice expansion (Doughty et al., 2015; García et al., 2018; Darvill et al., 2015, 2016). Evaluating the drivers of these pre-LGM advances and their role throughout the last glacial cycle is, however, limited by a lack of dated moraines spanning the entire glacial period. Moraine preservation is inherently incomplete due to a range of

erosional processes, including the removal of pre-existing moraines by an advancing glacier. As a result, moraine preservation in a landscape is biased toward the most extensive and the more recent glacial advances. Here, we present a ^{10}Be-dated chronology from the Lago Belgrano valley on the eastern side of Monte San Lorenzo (47.6° S, 3706m) in central Patagonia, Argentina, where a unique topographic setting has allowed preservation of a moraine record from the early stages of glaciation.

2. Physical setting

Monte San Lorenzo is an isolated granitoid massif that is situated ∼90 km east of the main spine of the Andes on the border with Chile (Chilean name: Monte Cochrane) (Fig. 1). At this latitude, faulting has created a topographic depression that breaks the main chain of the Andes (Lagabrielle et al., 2004) to separate the North Patagonian Icefield (NPI) from the South Patagonian Icefield (SPI), and the San Lorenzo massif from the Pacific coast. The Río Baker and Río Pascua exploit this ∼80 km gap in the mountain chain to drain much of the eastern side of the Andes, including the large cross-border lakes of Lago General Carrera/Buenos Aires (LBA), Lago Cochrane/Pueyrredón (LP), and Lago O'Higgins/San Martín (SM), westward to the Pacific Ocean. The San Lorenzo and southern massifs constitute an area of high topography stepped east of the main Andean chain (Fig. 1 C). They are enclosed on their southern, western and northern sides by deep glacial valleys, some of which have been eroded to below sea level (e.g. LP and LBA; Murdie et al., 1998). By comparison, their eastern side is less affected by glacial erosion. Lago Belgrano lies at over 800 m asl. and Lago

Burmeister at 900 m asl. The modern drainage divide runs just east of Lago Belgrano (Fig. 1 C), with this lake and the eastern outlet glaciers of San Lorenzo draining via a series of interconnected lakes westward into the Pacific Ocean. Lago Burmeister and the eastern part of the Belgrano valley instead drain eastward into the Atlantic Ocean via the Río Belgrano.

The geology of the area comprises Paleozoic basement rocks, intruded and overlain by Jurassic volcanic rocks and sedimentary sequences of Cretaceous and Jurassic age (Ramos et al., 1982; Ramos and Kay, 1992). The eastern part of the Belgrano valley is mainly characterized by Neogene and Paleogene volcanic sequences, the latter is represented by the Meseta Belgrano, which separates the Belgrano and Pueyrredón valleys (Ramos et al., 1982; Ramos and Kay, 1992). Monte San Lorenzo is part of the Patagonian Batholith intrusion, and is the nearest source of granitic boulders.

The climate of Patagonia is dominated by the SWW, which deliver precipitation to the present glaciers and icefields. The SWW are strongest during austral summer with the core situated between $45° - 55°$ S. In winter, they weaken and expand equatorward (Garreaud et al., 2009). The Andes create an orographic barrier to the westerly storms resulting in a strong west-east precipitation gradient. On the Pacific coast, precipitation reaches 5000 - 10 000 mm a^{-1} (Garreaud et al., 2013). East of the mountain divide precipitation decreases sharply to less than 300 mm a^{-1} within tens of kilometres from the mountain front (Garreaud et al., 2013). Air temperatures do not exhibit such a strong west-east gradient, and are pre-dominantly controlled by the SWW (Kilian and Lamy, 2012).

The San Lorenzo massif, situated about 160 km from the Pacific coast,

has a transitional maritime to continental climate (Falaschi et al., 2013). At this latitude, Monte San Lorenzo is the first orographic barrier to the SWW, which sustain this easternmost extensively glaciated area in the region (Falaschi et al., 2013). Glaciers of Monte San Lorenzo and the surrounding mountains cover an area of $\sim$207 km^2 (Falaschi et al., 2013). The snowline is estimated to be $\sim$ 1700 m asl on the western side and about 100 m higher on the eastern side of San Lorenzo (Falaschi et al., 2013). Glaciers of central Patagonia can be characterized as warm and wet, and are considered particularly sensitive to temperature changes (Sagredo and Lowell, 2012).

During the last glacial period, several tributary glaciers draining the San Lorenzo and southern massifs coalesced and flowed down the Belgrano valley (here referred to as the Belgrano glacier). By comparison with other outlets glaciers in central Patagonia, the Belgrano glacier was considerably smaller and occupied a relatively high-altitude valley. Three main moraine systems exist in the valley east of Lago Belgrano. Based on local landmarks, we informally name these moraine belts, Klementek, Menelik and Belgrano from the oldest to the youngest (Fig. 2). Here, we focus on the Klementek and Menelik moraine systems.

3. Glacial history and previous work

3.1. Previous work at Lago Belgrano

The glacial history of the Belgrano valley has received little scientific attention and is therefore largely unknown. Even Caldenius (1932), who mapped nearly all of Patagonia in his pioneering work, did not map the Belgrano valley. The area of Lago Belgrano was included in a Patagonia-wide

glacial geomorphological map (Glasser et al., 2008), and partly covered by a more detailed geomorphological mapping by Bendle et al. (2017b). The only field-based mapping and chronological work in the Belgrano valley was done by Wenzens (2005) and Horta et al. (2017). Wenzens (2005) documented the glacial geomorphology of the valley and tentatively correlated the outermost moraine belt (the Klementek Moraines) to the LGM. He attributed the Menelik moraine system to the Late Glacial based on a radiocarbon age of 14.85 ± 0.12 ^{14}C ka from a kettle hole (18.0 ± 0.2 cal ka BP [1]). Horta et al. (2017) focused on the palaeolake history and obtained radiocarbon ages from lacustrine sediments inboard of the Menelik moraines. The Late Glacial and Holocene glacier history has been investigated by several workers, mainly on the western and northern flanks of Monte San Lorenzo (Mercer, 1968; Davies et al., 2018; Glasser et al., 2012; Sagredo et al., 2017, 2018; Martin et al., 2019).

3.2. Pre- gLGM glacial history of Patagonia

In Patagonia, the evidence for pre-gLGM ice expansion is largely restricted to Marine Isotope Stage (MIS) 3 and earlier glacial cycles. In southern Patagonia ($49° - 55°$ S), several studies indicate MIS 3 advances that were significantly more extensive than the MIS 2 advances. On Tierra del Fuego (53-54° S), Darvill et al. (2015) determined that the Bahía Inútil - San Sebastián ice lobe advanced at 45.6 ($+139.9/-14.3$) ka and 30.1 ($+45.6/-23.1$) ka, and was up to 100 km more extensive than the subsequent gLGM lim-

[1] Recalibrated using the OxCal online calibration program (version 4.3; Bronk Ramsey, 2009) and the SHCal13 calibration curve (Hogg et al., 2013)

its (Kaplan et al., 2004; McCulloch et al., 2005). The Torres del Paine and Última Esperanza outlet glaciers (50° S) reached their maximum at 48.0 ± 1.6 ka with subsequent advances at 39.2 ± 2.0 ka and 34.0 ± 1.3 ka dated by ^{10}Be exposure ages (García et al., 2018; Sagredo et al., 2011). Here, the MIS 2 ice advances (21.5 ± 1.8 ka) were half the extent of the MIS 3 maximum (García et al., 2018). Tentative exposure dates from the San Martin valley (49° S) follow a similar pattern (Glasser et al., 2011).

In northern Patagonia ($40° - 44°$ S), glaciers also advanced during MIS 3 and MIS 2, but in contrast to southern Patagonia, the relative magnitudes were similar. In the CLD, stratigraphic evidence and radiocarbon chronology suggest ice expansion at $33.6 \sim 0.2$ ka, but this was similar in magnitude or smaller than later advances (Denton et al., 1999a; Moreno et al., 2015). Zech et al. (2011) reported an advance at 39° S on the eastern side of the Andes dated by ^{10}Be at $\sim$ 39 ka. Much of the glacial deposits on the eastern side of the Andes in northern Patagonia remains undated, which precludes firm conclusions on the magnitude and timing of the maximum ice expansion in the north.

In central Patagonia ($44° - 49°$ S), two chronologies from large former outlet glaciers suggest maximum ice expansion roughly during the gLGM, between $\sim$ 27 - 25 ka at LBA (Kaplan et al., 2004; Douglass and Bockheim, 2006), and $\sim$ 28 ka and perhaps $\sim$ 35 ka at LP (Hein et al., 2010, 2009). In both valleys, moraines outboard of the MIS 2 limits pre-date the last glacial cycle (Kaplan et al., 2005; Hein et al., 2017, 2009). Smedley et al. (2016) identified MIS 3 advances at LBA (34.0 ± 6.1, 30.8 ± 5.7 ka) using optically stimulated luminescence (OSL) dating of buried outwash sediment.

However, there are no preserved moraines related to this advance, which likely only reached to within the MIS 2 limits.

More widely, robust ^{10}Be chronologies from New Zealand indicate glacial advances at $\sim$ 42 ka (Pukaki valley, Kelley et al., 2014), $\sim$ 35.5 ka (Pukaki valley, Doughty et al., 2015) and $\sim$ 32 ka (Ohau valley, Putnam et al., 2013). Overall, ice expansion during MIS 3 appears to be a regional phenomena (Darvill et al., 2016). Despite this, we are still far from fully establishing the magnitude of the MIS 3 glacial expansion throughout Patagonia and its climatic significance.

Chronostratigrahic evidence for glacial expansion prior to MIS 3 in Patagonia is fragmentary. At the time of publishing, there are no firmly dated glacial advances during MIS 4 or 5. In the Chilean Lake District (CLD), the outermost moraine belts of three outlet lobes have been tentatively assigned to MIS 4 (Denton et al., 1999b; Heusser et al., 1999; Mercer, 1976) but this assignment is not based on firm geochronological data. Palaeoclimate proxies from the southern mid-latitudes (e.g. Kaiser and Lamy, 2010) and Antarctica (Johnsen et al., 1972; EPICA Community Members, 2004) indicate cold conditions comparable to the gLGM during MIS 4. Dust fluxes to Antarctica (Lambert et al., 2008) and the Southern Ocean (Martínez-Garcia et al., 2011), which are considered a proxy for glacial activity in Patagonia (Sugden et al., 2009; Kaiser and Lamy, 2010), suggest expansion of Patagonian glaciers at the time. It is likely that MIS 4 glacial records exist in Patagonia, but they have not yet been firmly dated. By comparison, in New Zealand, full glacial conditions during MIS 4 are well documented (e.g. McCarthy et al., 2008; Shulmeister et al., 2018; Schaefer et al., 2015). The only

tentative evidence for ice expansion in Patagonia during MIS 5 comes from two individual ^{10}Be ages (91.4 ± 4.1 ka, 96.8 ± 4.8 ka) from Lago San Martin (49° S; Glasser et al., 2011). As a consequence, little is known about the development of the Patagonian Ice Sheet (PIS) from the onset of the last glaciation towards the gLGM.

4. Methods

4.1. Geomorphic mapping

Geomorphological mapping was done using high resolution imagery (2.5 m to sub-meter) available through the ESRI^{TM} World Imagery service, along with 10 m Sentinel-2 imagery. An ALOS PALSAR radiometrically terrain-corrected digital elevation model with a resolution of 12.5 m was used to aid landform identification. Geomorphological features were identified and mapped following well established criteria (Glasser et al., 2008; Bendle et al., 2017b; Darvill et al., 2014; Martin et al., 2019). Mapping was supported by ground-truthing during two field campaigns in the austral summers of 2016 and 2018.

4.2. Dating approach and sampling

Cosmogenic nuclide surface exposure ages from glacial boulders are commonly used to establish the timing of glacial advances/still-stands in a range of environmental settings (e.g. Heyman et al., 2011). The technique works well in most settings on timescales relevant to the gLGM, but it can break down on older moraine systems due to site specific environmental factors that can affect nuclide concentrations, such as moraine degradation and boulder

erosion (Putkonen and Swanson, 2003; Hallet and Putkonen, 1994; Briner et al., 2005; Hein et al., 2009, 2017; Heyman et al., 2011; Gillespie and Bierman, 1995; Applegate et al., 2010). Depending on the environmental conditions, direct dating of glaciofluvial outwash sediments directly linked to a moraine system can circumvent some of these issues to be an effective way of constraining the timing of a glacial advance. This is because outwash terraces are flat, unlike moraine ridges, and less susceptible to gravity-driven surface lowering, which minimises the potential for exhumation of surface clasts. Furthermore, the outwash cobbles rooted in the terraces are subject to less wind erosion, which is a significant source of boulder erosion in Patagonia. The outwash method has proved effective at dating pre-LGM glacial advances as old as one million years in this region (Hein et al., 2009, 2011, 2017; Darvill et al., 2015; Cogez et al., 2018). To develop our chronology, we measured cosmogenic ^{10}Be in both moraine boulders and glacio-fluvial outwash cobbles.

To date the Menelik moraines, we sampled six boulders on the outermost moraine ridges, one boulder on the inner moraine and two samples came from moraines near the northern valley side. In addition, we sampled five cobbles from its associated outwash terrace. To date the Klementek system, we sampled six surface cobbles from two sites on the outwash terrace associated with the outermost moraines. Surface boulders on this moraine system are rare; those we found were significantly eroded and unsuitable for dating. The sample details are presented in Table 1. When sampling, we preferentially targeted large (ideally >1 m) stable boulders on moraine crests that showed minimal signs of surface erosion (cf. Heyman et al., 2016; Putkonen

and Swanson, 2003). Samples were collected by hammer and chisel from the centre of the boulder surface (Gosse and Phillips, 2001; Darvill, 2013). Outwash cobbles were collected whole from locations where the outwash terrace could be unambiguously linked to the moraine system, but far enough from the moraine ridges to avoid material transported down its slopes and onto the terrace surface (Hein et al., 2011, 2009).

4.3. Preparation

Samples were prepared at two cosmogenic nuclide laboratories: the Natural Environment Research Council's Cosmogenic Isotope Analysis Facility (NERC-CIAF) and the University of Edinburgh's Cosmogenic Nuclide Laboratory. The samples were crushed, milled and then sieved to obtain the 250 μm to 500 μm (CIAF), or 250 μm to 710 μm (Edinburgh) size fraction. Large cobbles (>10 cm) were cut to an appropriate thickness parallel to the surface prior to crushing, while the majority of the cobbles were fist-sized and these were crushed whole. All measurements of ^{10}Be concentrations were done at the Scottish Universities Environmental Research Centre (SUERC) Accelerator Mass Spectrometry (AMS) facility.

4.3.1. NERC-CIAF Preparation

The 250 μm to 500 μm fraction was magnetically separated using a Franz machine and the non-magnetic fractions were recovered. To remove carbonates and soluble oxides, the samples were first treated with a 6:1:1 solution of water, HCl (37%) and HNO_3 (68%, aqua regia), on a hot-plate ($\sim 50°C$) and the supernatant was discarded. The samples were then treated with a 100:1 mixture of water and concentrated (40%) HF on a shaker table for one

hour to slightly etch feldspar and mica grain surfaces. Supernatant liquid was discarded. Feldspar and mica minerals were then removed through froth floatation (Herber, 1969): the samples were repeatedly treated with eucalyptus oil, to make the etched grains hydrophobic, and a carbonated surfactant solution. Floating minerals were then discarded and quartz grains that did not float were recovered. The samples were then etched three times in a 1 litre solution of water, HF (40%) and HNO_3 (150:2:1) in a high power ultrasonic tank to isolate the cores of the quartz grains. An aliquot of the final quartz sand was dissolved and its purity was tested for Al, Be, Fe, Ca and Ti by ICP-OES at SUERC. The samples were dissolved in pure HF and each sample and process blanks (n=2) were spiked with $\sim$ 0.2 mg of ^{9}Be carrier. After dissolution, the HF was evaporated and replaced by HCl. The solutions were first passed through anion exchange chromatography columns to remove Fe. The Fe-free fraction was then evaporated and the HCl was replaced by diluted H_2SO_4. The sulphate solutions were then passed through cation exchange chromatography columns to remove Ti and B, and to separate Be and Al fractions. The ^{10}Be fractions were precipitated as hydroxides and oxidised at $\sim 900°C$. Resulting BeO were mixed with Nb (1:6) and pressed into copper cathodes for AMS analysis. All measurements were normalized to NIST SRM4325 standard with nominal ratios of 2.79×10^{-11} $^{10}Be/^{9}Be$ (Nishiizumi et al., 2007) and half-life of 1.36 Ma. The blank corrections ranged between 1 and 4% of the sample $^{10}Be/^{9}Be$ ratios.

4.3.2. Edinburgh Preparation

At the University of Edinburgh's Cosmogenic Nuclide Laboratory, quartz was isolated through repeated acid etching following standard procedures (Nishiizumi et al., 2007; Bierman et al., 2002). The samples and the process blanks (n=2) were spiked with $\sim$ 0.25 mg ^{9}Be carrier. The samples were prepared as BeO targets for AMS analysis following procedures detailed by Hein (2009), which are similar to those described above. $^{10}Be/^{9}Be$ measurements were normalized to the standards of Nishiizumi et al. (2007) with nominal ratios of 2.79×10^{-11}. The blank corrections were under 1% of the sample $^{10}Be/^{9}Be$ ratios.

4.3.3. Age Calculations

The ^{10}Be ages were calculated using the online exposure age calculator formerly known as the CRONUS-Earth online calculator (version 3, Balco et al., 2008), with the Patagonia production rate (Kaplan et al., 2011) obtained from the ICE-D online database (`http://calibration.ice-d.org/`). Throughout the paper we report ages calculated using the time-dependent scaling scheme of Lal (1991) modified by Stone (2000). Using the New Zealand ^{10}Be production rate (Putnam et al., 2010), our ages decrease by less than 1%, and using the global production rate (Borchers et al., 2016) the ages decrease by $\sim$ 6%. Summary statistics for each moraine system are provided in Table 2. We base our discussion on the arithmetic mean and 1 σ standard deviation for each moraine system.

The ages presented here assume zero erosion and are therefore minimum ages. Topographic shielding was measured in the field and is negligible for all samples ($\sim$ 0.99). The ages are not corrected for snow, vegetation or

soil shielding. Vegetation is sparse in the area, mostly comprises steppe grasses and is unlikely to introduce significant shielding. Owing to high winds and the semi-arid environment, we expect snow shielding to be minimal. Soils in the field area are thin (normally 0-10 cm) and spatially variable, and a significant lag is expected before soil develops following ice retreat. Quantifying soil shielding over the exposure history is therefore difficult, but we expect the impact on ages to be minimal.

5. Results

5.1. Moraine Record

The Klementek moraine system comprises of well-defined outermost moraine ridges with 25 m relief and slopes up to 12° deposited in the eastern part of the valley, $\sim$ 65 km from present day glacier margins (Fig. 2). The outermost moraine ridges are discontinuous and up-valley transition into a hummocky terrain, which extends for 10 km on the northern side of the Río Belgrano (Fig. 3). Hummocks and hollows are interspersed with streamlined, ice-flow parallel landforms of 250 - 450 m in length. Small narrow ridges of up to one kilometer in length, perpendicular to former ice flow, are superimposed on the hummocky terrain, and are interpreted as recessional moraines. Occasional, significantly eroded boulders with fluting and ventifacts are scattered on the hummocky terrain. A glacio-fluvial outwash terrace emanates from the distal margin of the outermost moraine ridges. Relict braided channels can be traced from the surface of the outwash to the moraines. The outermost moraine ridges are interpreted to mark a former ice margin position of the Belgrano glacier, while the hummocky terrain was likely formed by a

combination of subglacial and ice-marginal processes during ice retreat. The morphology of the Klementek moraine system is suggestive of a pre-LGM age.

The Menelik moraines (Fig. 4 and 5) are 22 km up valley and are separated from the Klementek moraines by a >10 km long broad glacio-fluvial outwash terrace. The double-lobate shape of the Menelik moraines and the presence of a medial moraine indicate the coalescence of the Belgrano and Burmeister glaciers. The outermost Menelik moraines are prominent, cross-valley ridges with broad crests, and 30 m relief and slopes up to 15° (Fig. 4 and 5). Clusters of exposed gravel and abundant boulders can be found on moraine crests. Inboard, moraines diminish in size and in places are interspersed with numerous ponds and depressions. Numerous small (1-2 m relief) moraine ridges are preserved on higher ground (Fig. 4 A). The sequence of smaller moraines extends up valley over a distance of $\sim$ 10 km, and suggests deposition during ice recession. Palaeoshorelines indicate formation of shallow proglacial lakes as the ice margin retreated (Fig. 2). Near the northeast shore of Lago Belgrano, the Menelik moraines are cross-cut by the younger Belgrano moraines (Fig. 2). This indicates that the glacier retreated into the Belgrano trough prior to a subsequent re-advance, which also removed part of the inner Menelik moraine system. Glacio-fluvial outwash terraces emanate from the Menelik moraines with preserved relict surface channels. The outwash plain has been incised by two rivers, leaving the area sampled isolated and unaffected by post deposition fluvial processes.

5.2. Exposure ages

We present 20 new exposure ages from the Klementek and Menelik moraine systems. The ^{10}Be data are presented in Figures 3 B and 5, and Tables 1-2. The probability density diagrams ('camelplots') are shown in Figure 6. In the following, we report individual ^{10}Be ages with 1 σ internal uncertainties.

The ages from the Klementek outwash range from 67.1 ± 1.7 ka to 85.9 ± 1.9 ka (n = 6; Fig. 3 B and 6 A). The distribution of ages contains a cluster of four ages, with one younger and one older age. The ages yield a mean of 75.7 ± 5.9 ka (all data), or 75.2 ± 2.8 ka with the outliers excluded.

The boulder ages from the Menelik outermost moraines range from 18.4 ± 0.6 ka to 26.0 ± 0.8 ka (n=6; Fig. 5 and 6 B). We consider the youngest sample (18.4 ± 0.6 ka) an outlier because it was taken from a short, partly buried boulder and was likely exhumed from the moraine matrix post-deposition. The remaining samples range from 23.0 ± 0.6 ka to 26.0 ± 0.8 ka and yield a mean age of 24.8 ± 1.1 ka. The two boulders from moraines near the Belgrano valley side yielded ages of 22.9 ± 0.9 and 18.3 ± 0.6 ka. The boulder from the inner Menelik moraine gave an age of 17.0 ± 0.7 ka. Cobble ages from the Menelik outwash (Fig. 5 and 6 C) range from 23.7 ± 0.9 ka to 26.0 ± 1.0 ka, excluding an older age of 36.6 ± 1.1 ka, and yield a mean age of 24.8 ± 0.9 ka.

6. Discussion

6.1. The age of the Klementek outwash

6.1.1. Geomorphic considerations

The distribution of the Klementek outwash cobble ages suggests that the samples may have been affected by pre- and post-depositional processes. One possibility is that the cobbles are erroneously young because they were exhumed through bio- or cryo-turbation, or as the terrace surface lowered through time. We do not expect bio- or cryo-turbation processes to significantly affect the exposure ages because soils at the site are thin, which should limit this process. Terrace deflation is also expected to be insignificant based on a study in the neighboring Lago Pueyrredón valley to the north. Here, Hein et al. (2009) estimated outwash terrace surface lowering rates at 0.53 mm ka^{-1} using a depth-profile approach. This rate would imply about 45 mm of total terrace surface lowering over the past 86 ka (the age of oldest outwash sample), which would not significantly decrease the apparent exposure ages. Rock surface erosion is another potential source of geological scatter and erroneously young apparent exposure ages. Our ages assume no rock surface erosion, but minor surface erosion is evident on most Klementek cobble samples (Fig. 3 F). The erosion depth is variable but less than $\sim$ 3 mm (Figures 3 F). This amount of erosion integrated over $\sim$ 86 ka (age of oldest sample) yields an erosion rate of 0.035 mm ka^{-1}. Applying this erosion rate to the age calculations would increase the ages by less than 1 %, which is within the analytical uncertainty.

Nuclide inheritance is a potential source of geological scatter that would make the ages erroneously old. We assume inheritance is negligible because

the outwash sediment was shielded, transported and eroded by warm-based ice before deposition. This assumption is supported by depth-profile measurements in the neighbouring Lago Puyerredón valley where average inheritance was demonstrated to be negligible (Hein et al., 2009), and by the similarity of outwash cobble and moraine boulder exposure ages. Given the similarity of ages obtained from the Menelik moraine boulders and outwash surface cobbles, we too conclude inheritance is low.

6.1.2. Age interpretation

There are several ways to interpret the outwash exposure ages: 1) If we assume that the oldest sample remained on the surface the longest and the other samples were exhumed later as the outwash terrace deflated, then the oldest age approach (cf. Hein et al., 2009) would provide the closest age for the deposition of the outwash at $\sim$ 86 ka. 2) The youngest and oldest ages were affected by pre- (85.9 $\pm$ 1.9 ka, e.g. inheritance) and post-depositional processes (67.1 $\pm$ 1.7 ka, exhumation). If we exclude them as outliers, we obtain a mean age of 75.2 $\pm$ 2.8 ka (n=4), which would be the best possible age for the deposition of the outwash. 3) All ages are correct and the outwash is of composite age, and was deposited during ice expansion between $\sim$ 86 and 67 ka. Given the clustering of ages and our assessment of the significance of terrace deflation, exhumation and inheritance, we tentatively suggest the mean age of 75.2 $\pm$ 2.8 ka (scenario 2) as the best estimate for the culmination of the ice advance that deposited the outwash. However, since we cannot exclude other scenarios, we acknowledge that the outwash might be as old as 86 ka or it could have been deposited between 86 - 67 ka.

Our mapping suggests the Klementek moraines are age-equivalent to the

dated outwash and therefore represent a glacial advance at 75.2 ± 2.8 ka ka; the morphology of the moraine system is consistent with this age. We acknowledge that the hummocky terrain with superimposed moraine ridges could be a palimpsest feature younger than the dated outwash and could have been deposited during MIS 4 and 3.

6.2. The age of Menelik moraines and outwash

The Menelik outermost moraine boulders yield a mean age of 24.8 ± 1.1 ka, excluding one young outlier. The outwash cobbles yield a mean age of 24.8 ± 0.9 ka, excluding one older outlier. As with the Klementek outwash, there are several ways to interpret the Menelik outwash ages: 1) the oldest age approach (36.6 ± 1.1 ka, LB1623); 2) the oldest age is an outlier (e.g. contains inherited nuclides or reworked from previous advance) 3) all ages are correct, and the outwash is of composite age. The relative clustering of the boulder and outwash ages indicates that scenario 2) is most likely. Our field observations, however, provide some support for scenario 3, since there is a remnant of a smaller moraine just outboard of the outermost Menelik moraine sampled. It is possible the oldest outwash sample (36.6 ± 1.1 ka) represent this earlier, slightly more extensive advance, and therefore we tentatively suggest an advance at this time. The remaining four samples, which produce a central peak (Fig. 6 C), would therefore relate to the major advance that deposited the prominent outermost moraines and (part-) deposited the outwash. Excluding two ages (LB1618 and LB1623), the remaining outwash and moraine boulder exposure ages are indistinguishable and when combined together yield a mean age of 24.8 ± 1.0 ka, which we interpret as the timing of this major advance.

6.3. The last glacial cycle at Lago Belgrano

Our ^{10}Be ages suggest the most extensive advance of the Belgrano glacier occurred early in the last glacial cycle at 75.2 ± 2.8 ka ka toward the end of MIS 5. Given the scatter in our exposure ages and the extent of the hummocky terrain with recessional moraines, it is possible the glacier oscillated near its maximum position between 86 - 67 ka. The advance precedes major cooling during MIS 4, when some New Zealand glaciers had reached full glacial conditions (e.g. McCarthy et al., 2008; Shulmeister et al., 2018; Schaefer et al., 2015). Whilst we find no unambiguous evidence for an advance during MIS 4, we recognize the youngest age of 67.1 ± 1.7 ka overlaps in timing. We only dated outwash associated with the outermost moraines, it is therefore possible that some of the recessional moraines were deposited during MIS 4.

We have tentative evidence for an advance during MIS 3 (36.6 ± 1.1 ka), but this requires further chronological constraint. Significant MIS 3 glacial advances have been identified at several locations elsewhere in Patagonia (Darvill et al., 2015; Smedley et al., 2016; García et al., 2018; Denton et al., 1999b). A second major, but considerably smaller, advance of the Belgrano glacier is represented by the Menelik moraines and occurred at 24.8 ± 1.1 ka, coeval with the gLGM.

6.4. Evidence for MIS 5 glaciation

The Belgrano glacier reached its maximum extent much earlier than elsewhere in Patagonia, where MIS 3 is the more dominant signal. Our data provide the first robust evidence for MIS 5 glaciation in Patagonia. Elsewhere in the southern mid-latitudes, evidence for MIS 5 glaciation is fragmentary. In

southern Patagonia, the maximum expansion of the Lago San Martin outlet glacier may have occurred during late MIS 5 (Glasser et al., 2011). In New Zealand, ^{10}Be ages from the Cascade valley, suggest an advance at $\sim$ 90 ka (Sutherland et al., 2007). Shulmeister et al. (2010) reported glacier advances at $\sim$ 100 - 90 ka and $\sim$ 80 ka in the Rakaia Valley based on stratigraphic evidence and OSL ages. The advance of Belgrano glacier could correlate with ice expansion evident in New Zealand during MIS 5b-a.

In the northern hemisphere, there is evidence for expansion of mountain glaciers and ice sheets during MIS 5. For example, glaciers in central Asia (Röhringer et al., 2012; Koppes et al., 2008), NE Siberia (Zech et al., 2011), as well as in NW Washington and in the Pyrenees (Pallàs et al., 2010; Lewis et al., 2009) reached their maximum during MIS 5. Sectors of large northern hemisphere ice sheets expanded to their maximum position early in the last glacial cycle. For example, the Barents-Kara ice sheet reached its maximum extent during MIS 5 (90 - 80 ka), and was less extensive during subsequent glaciations (Svendsen et al., 2004).

These studies demonstrate substantial glaciation of mid-latitude mountain areas globally, as well as the growth of ice sheets, during MIS 5. Our data demonstrates extensive glaciation of the eastern massifs of central Patagonia at this time. We speculate that the onset of glaciation throughout the Patagonian Andes also occurred during MIS 5, but the geomorphic and stratigraphic evidence has largely been destroyed, or remains undiscovered.

6.5. gLGM and deglaciation in Patagonia

Our data show that the Belgrano glacier advanced at 24.8 $\pm$ 1.0 ka during the gLGM, but this advance was substantially smaller than the MIS 5

advance. The timing of this advance is in good agreement with other glacial records in Patagonia (e.g. Hein et al., 2010; Kaplan et al., 2004, 2008; McCulloch et al., 2005; Denton et al., 1999b). For example, in central Patagonia, the LP outlet glacier achieved its maximum extent at $\sim$ 28 ka with a subsequent advance at $\sim$ 25 ka (Hein et al., 2010). The LBA outlet lobe was at its maximum at $\sim$ 27 - 25 ka followed by several smaller re-advances/still-stands (Kaplan et al., 2004; Douglass and Bockheim, 2006). Advances during the gLGM in southern Patagonia were substantially less extensive than the MIS 3 advances (García et al., 2018; Darvill et al., 2015; McCulloch et al., 2005; Kaplan et al., 2008).

The presence of numerous, regularly spaced recessional moraines indicate that deglaciation from the 25 ka limits at Lago Belgrano was, at least initially, gradual. We speculate that the Belgrano glacier occupied the eastern portion of the valley for at least 8 ka, between $\sim$ 25 ka and $\sim$ 17 ka, based on the age from the inner Menelik moraine (17.0 $\pm$ 0.7 ka), but further work is needed to confirm this. Shallow proglacial lakes formed as the ice margin retreated from the inner Menelik moraines. Once the glacier retreated into the Belgrano trough, it likely experienced a more dynamic retreat associated with calving. We have no evidence to constrain the maximum recession prior to the re-advance that deposited the Belgrano moraines.

Although we cannot firmly constrain the timing and rate of deglaciation, our youngest age (17.0 $\pm$ 0.7 ka) from the inner Menelik moraine broadly matches the onset of deglaciation elsewhere in Patagonia. At LP, deglaciation began as ice withdrew from the youngest Río Blanco moraines dated at $\sim$ 21 - 19 ka (Hein et al., 2010). Rapid deglaciation of the LP and Chacabuco

valleys accompanied by ice thinning is supported by a vertical reconstruction (Boex et al., 2013) and a pollen analysis of a lake core (Henríquez et al., 2017). At LBA, the onset of deglaciation was dated at 18.1 ± 0.2 ka, followed by a short still-stand at 17.7 ± 0.1 ka, which deposited the Menucos moraines (Bendle et al., 2017a; Kaplan et al., 2004; Douglass and Bockheim, 2006). Deglaciation was initially steady, but accelerated after 17.3 ka when the LBA outlet lobe started to calve into a deep lake (Bendle et al., 2017a). Overall, it appears that in central Patagonia deglaciation was underway by 19 - 18 ka (García et al., 2019; Markgraf et al., 2007; Hein et al., 2010; Henríquez et al., 2017; Bendle et al., 2017a), while in southern Patagonia and in the CLD ice retreat initiated about 1 ka later (McCulloch et al., 2005; García et al., 2014; Kaplan et al., 2008; Sagredo et al., 2011; Denton et al., 1999a; Moreno et al., 2015; Mendelova et al., 2017).

6.6. Causes of glaciation

In the following we consider potential mechanisms that could lead to ice expansion during MIS 5 and the pattern of successively smaller ice extent at Lago Belgrano.

6.6.1. Insolation

Earth's orbital parameters exert a primary control on glacial-interglacial cycles and modulate global climate (Hays et al., 1976; Milankovitch, 1941). Insolation in the southern hemisphere is almost completely out-of-phase with the northern hemisphere, and it has been proposed that southern hemisphere insolation modulates regional climates, and therefore controls glacial advances in the southern mid-latitudes (Vandergoes et al., 2005; Sutherland

et al., 2007; Darvill et al., 2015, 2016).

A minimum in southern hemisphere summer insolation occurred between 85 - 75 ka (Fig. 7 B), and this may have promoted ice advance at Lago Belgrano. As noted by Hughes and Gibbard (2018), insolation played a particularly important role in glacial inception, including the insolation minimum at the end of the previous interglacial. The amplitude of southern hemisphere insolation change is greatest during MIS 5, with a minimum of the last glacial cycle between 115 ka and 100 ka. This would have likely created favorable conditions for glaciation of the Patagonian Andes. Glaciers in mid- and high-northern latitudes are thought to have expanded in response to reduced summer insolation early in the last glacial cycle (e.g. Abramowski et al., 2006; Porter and Swanson, 2008; Farquharson et al., 2018).

Reduced southern hemisphere summer, as well as winter, insolation have been invoked to explain glacier expansion in Patagonia and New Zealand during MIS 3 (Darvill et al., 2015, 2016; García et al., 2018). However, Doughty et al. (2015) and Darvill et al. (2016) noted that southern hemisphere insolation alone cannot explain the timing of glacier advances observed in the southern mid-latitudes. While insolation was important in driving the onset of glaciation, later in the glacial cycle it may have only played a comparatively minor role (Hughes and Gibbard, 2018). Further, variations in insolation would modulate regional climates differently (Gillespie and Molnar, 1995). The timing and extent of ice advances along the Patagonian Andes was then ultimately determined by local-to-regional factors and feedback mechanisms (cf. Darvill et al., 2016; García et al., 2018).

An alternative hypothesis suggests that the precessional cycle might af-

fect the timing of glacial advances in the southern mid-latitudes by controlling southern hemisphere seasonality and the pole-to-equator thermal gradient, which in turn drives westerly circulation (Shulmeister, 1999; Shulmeister et al., 2004). Glacial advances would therefore occur at southern hemisphere precessional maxima, i.e. 23 ka, 48 ka, 72 ka, and 96 ka (Shulmeister et al., 2010). In this model, ice expansion at Lago Belgrano might have been driven by a precessional maximum at 96 ka and at 72 ka. There is evidence for ice advances in Patagonia at $\sim$ 48 ka (García et al., 2018), and in NZ at $\sim$ 42 ka (Kelley et al., 2014) that could be linked to a precessional maximum at 48 ka.

6.6.2. Moisture availability

While the initial growth of the San Lorenzo ice cap was likely driven by reduced southern hemisphere insolation, we suggest the early maximum and successively smaller ice extent at Lago Belgrano was, in part, related to decreasing moisture delivery over the course of the glacial cycle. The San Lorenzo massif is the easternmost glaciated area in Patagonia today, sustained by westerly precipitation. Early in the glacial cycle, expansion of an independent ice cap over San Lorenzo would have been fostered by westerly precipitation that was able to penetrate through the gap in the Andes. Once the full PIS developed to the west, it blocked this gap and created a lee-side effect that led to a reduction in snowfall over San Lorenzo. As a consequence, the Belgrano glacier was substantially smaller during the gLGM.

Availability of moisture and the role of continentality has been highlighted as an important factor contributing to an early local LGM and a pattern of

successively smaller extent of mountain glaciers (Hughes and Gibbard, 2018; Gillespie and Molnar, 1995). For example, maximum glaciation of the mountain ranges in central Asia early in the glacial cycle was attributed to higher precipitation related to the strength and advection of the South Asian monsoon and/or westerlies (e.g. Röhringer et al., 2012; Dong et al., 2018; Zech, 2012; Owen et al., 2002; Finkel et al., 2003; Owen et al., 2003; Abramowski et al., 2006). Development of large northern hemisphere ice sheets would have affected atmospheric circulation and created lee side effects and precipitation starvation in other glaciated areas, thus indirectly contributing to a pattern of successively smaller glaciation elsewhere that was asynchronous with the global ice volume (e.g. Thackray, 2001; Porter and Swanson, 2008; Svendsen et al., 2004; Zech et al., 2011; Farquharson et al., 2018).

6.6.3. Antarctic stadials

On millennial time-scales, glacial advances in Patagonia and New Zealand have also been attributed to cooling in the southern mid-latitudes during Antarctic stadials (García et al., 2018; Kelley et al., 2014; Schaefer et al., 2015). An Antarctic millennial-scale climate signature across the southern mid-latitudes is likely an expression of antiphased interhemispheric coupling commonly attributed to the bipolar seesaw (Pedro et al., 2018; Stocker and Johnsen, 2003). Meridional oceanic heat transfer causes the Southern Ocean and Antarctica to cool during warm interstadial conditions in the North Atlantic region, and vice versa (Blunier, 2001; EPICA Community Members, 2006). Likely forced from the North Atlantic, the oceanic teleconnections are accompanied by an atmospheric reorganization (Markle et al., 2017; Buizert et al., 2018), which causes equatorward migration of the SWW during

Antarctic stadials (Markle et al., 2017; Lamy, 2004; Buizert et al., 2018). Further, the Antarctic Circumpolar Current weakens (Lamy et al., 2015), and cold water masses are advected northward resulting in lower SST off Chile (Kaiser et al., 2005) and New Zealand (Barrows et al., 2007). Together this could promote glacier expansion in Patagonia and New Zealand.

Antarctic millennial-scale climate variations have been correlated across the southern mid-latitudes by a range of marine proxies (e.g. Barrows et al., 2007; Lamy, 2004; Caniupán et al., 2011). Southern high- to- mid latitude millennial-scale cooling evident in Antarctic ice-cores and several marine records might have also facilitated the glacial advance at our site at $\sim$ 75 ka. Cold stadial conditions at this time are evident in Antarctic ice cores following the prolonged A7 warm event (7 F; Blunier, 2001; EPICA Community Members, 2006. A Mg/Ca-based SST reconstruction from east of New Zealand indicates a temperature decrease towards $\sim$ 75 ka (45° S, Pahnke et al., 2003; Fig. 7 D). Although the resolution of exposure dating and associated geological uncertainties do not allow for precise correlations, it is reasonable to expect that mountain glaciers in the southern mid-latitudes responded to such cooling events.

6.6.4. Build-up of the Patagonian Ice Sheet and ice-divide migration

In the light of the above discussion, we propose a conceptual model of the build-up of the PIS (Fig. 8). The San Lorenzo massif and surrounding high topography (and present day NPI and SPI) likely acted as nucleation points for the ice sheet. Ice inception here allowed for the development of an independent ice cap at the time of reduced southern hemisphere insolation and higher moisture availability early in the glacial cycle. Growth of the San

Lorenzo ice cap would have been sustained by westerly precipitation that was able to reach the eastern massif through the gap in the Andes (Fig. 8 A). Later in the glacial cycle, the individual ice masses that were building up on high topography, including the San Lorenzo massif, the NPI and the SPI, coalesced to form a continuous ice sheet (Fig. 8 B). Approaching peak glacial conditions (Fig. 8 C), we expect the ice-divide migrated westward towards the precipitation source, and in the process caused re-organization of ice-drainage routes to focus ice flow into the major outlets of the PIS that surround the San Lorenzo and southern massifs (LP and SM). Furthermore, increasing the ice-sheet elevation and migrating the ice-divide would create an effective barrier to westerly precipitation, causing a reduction in snowfall reaching the San Lorenzo massif (cf. Sugden et al., 2002). The successively smaller glacial extent of the Belgrano glacier can therefore be explained by reduced moisture on the lee side of the PIS and ice-drainage re-organization as a consequence of ice-divide migration. This explains why the Belgrano glacier was relatively small at $\sim$ 25 ka, at a time when the major regional outlets of the PIS (LP and LBA) were at their local maximum (Hein et al., 2010, 2009; Kaplan et al., 2004).

7. Conclusion

Our ^{10}Be ages and geomorphological mapping demonstrate that the Belgrano glacier reached its maximum extent of the last glacial cycle at $\sim$ 75 ka towards the end of MIS 5. A second, substantially smaller advance occurred at $\sim$ 25 ka during the gLGM. The topographic setting prevented overprinting of the MIS 5 moraine record by later advances. We suggest that an indepen-

dent ice cap developed over San Lorenzo early in the last glacial cycle, likely in response to reduced southern hemisphere summer insolation. Fostered by relatively high westerly precipitation, this led to the most extensive advance of the Belgrano glacier early in the last glacial cycle. Successively smaller ice extent at Lago Belgrano can be explained by snow starvation, ice-divide migration and ice-flow re-organization as the full PIS developed to the west of San Lorenzo. Our data provide first robust evidence for glaciation of the Patagonian Andes during MIS 5. However, more work is needed to elucidate the drivers of glaciation in Patagonia, from the onset early in the glacial cycle through to the full glacial conditions.

Acknowledgements

This work was supported by a NERC PhD studentship (NE/L002558/1) to MM. ^{10}Be analysis was supported by NERC CIAF grant (9167/0416). The British Society for Geomorphology, Quaternary Research Association, Royal Geographical Society (with IBG) and Explorers Club supported the 2018 field campaign. We also acknowledge funding from the Scottish Alliance for Geoscience, Environment and Society (Small Grants Scheme), and the Moray Endowment Fund from the University of Edinburgh. We are grateful to Andrew Gray for his help with fieldwork and Patricio Parada for arranging export of samples. The national park authorities of Argentina are thanked for granting permission to conduct fieldwork, and the rangers of the Perito Moreno National Park are thanked in particular for their assistance in the field. We would like to thank D. Sugden and R. McCulloch for insightful discussions. We are grateful for the constructive comments from five

anonymous reviewers that greatly improved this manuscript.

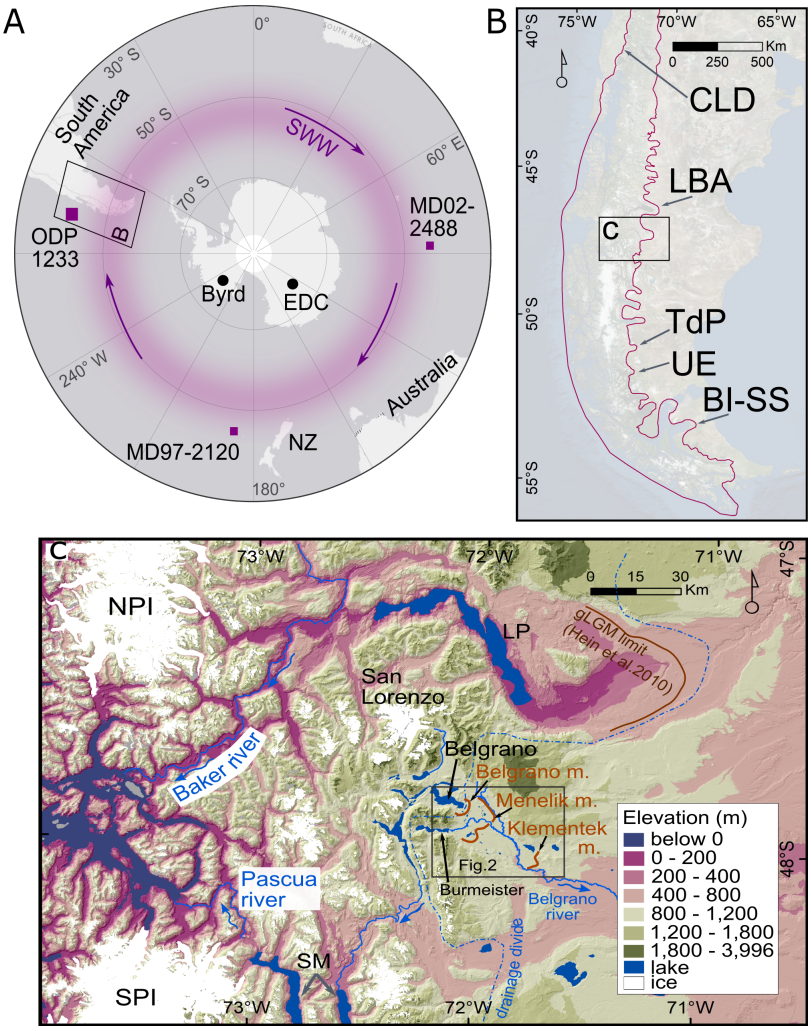

Figure 1

Figure 1: A) Location of Patagonia in the southern hemisphere along with Southern Ocean and Antarctic proxies discussed in the text and approximate location of the southern westerlies (SWW). B) Location of our study site in Patagonia and approximate extent of the Patagonian Ice Sheet during the gLGM (Singer et al., 2004). Image: ESRI World Imagery. (LBA: Lago Buenos Aires, TdP: Torres del Paine, UE: Última Esperanza, BI-SS: Bahí Inútil-San Sebastián lobe). C) The topography of central Patagonia including the tectonic gap that breaks the main chain of the Andes to separate the North Patagonian Icefield (NPI) from the South Patagonian Icefield (SPI), and the San Lorenzo massif (SL) from the Pacific Ocean (not shown). The Lago Belgrano study area is indicated. Blue arrows depict drainage directions described in the text, blue dotted line represents hydrological drainage divide. (LP: Lago Puyerredón, SM: Lago San Martín). The hillshade basemap was derived from the Shuttle Radar Topography Mission (SRTM) Digital Elevation Model (v3, 30m). Glacier outlines are from the GLIMS database (Falaschi et al., 2017; De Angelis et al., 2015).

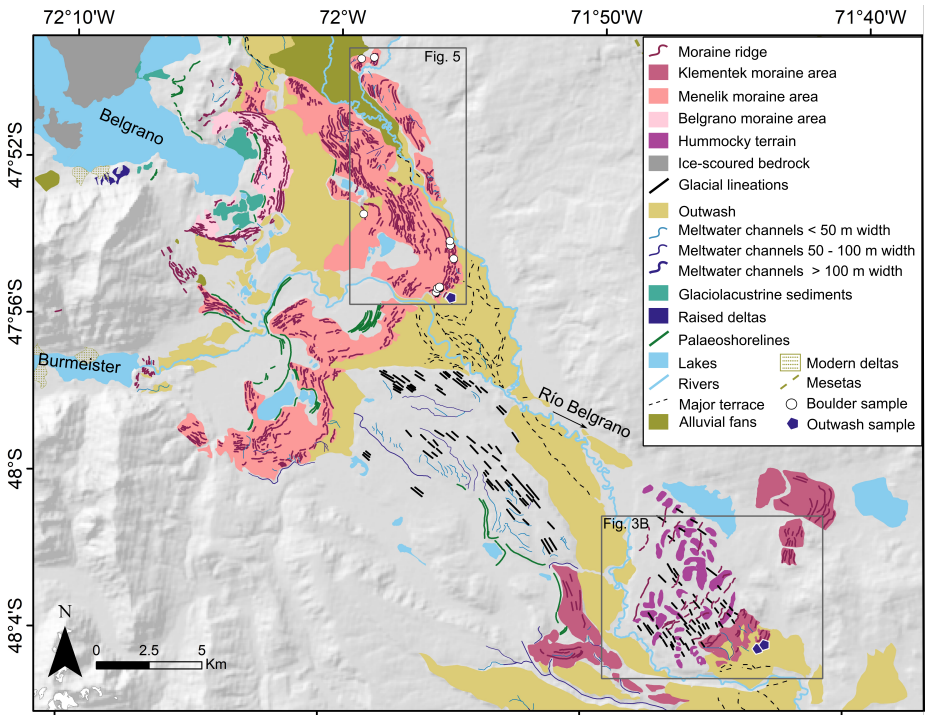

Figure 2: Geomorphological map showing the main moraine systems in the Belgrano valley, informally named the Klementek, Menelik and Belgrano moraines from the oldest to youngest. Sample locations are also shown. The hillshade basemap was derived from the Shuttle Radar Topography Mission (SRTM) Digital Elevation Model (v3, 30m).

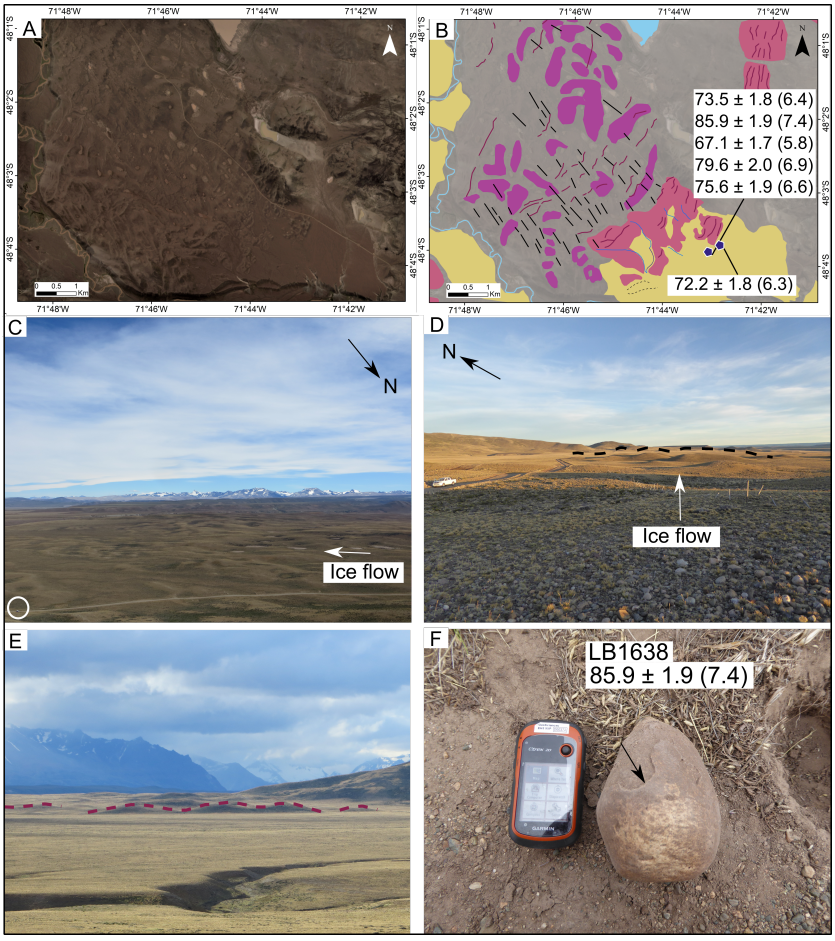

Figure 3: A) Satellite image (Sentinel-2) and B) mapped moraine ridges of the Klementek moraine system and the associated hummocky terrain. Sample locations and ^{10}Be exposure ages are also shown. C) Photograph showing part of the hummocky terrain, with a vehicle in the bottom left corner for scale. D) Photograph showing the outermost Klementek moraine ridges. E) Photograph showing the outermost Klementek moraine ridges and the associated outwash in foreground that was sampled for surface exposure analysis. F) An example of an outwash cobble sampled, which still exhibits fluvial shape, but some surface erosion is evident (maximum 3 mm).

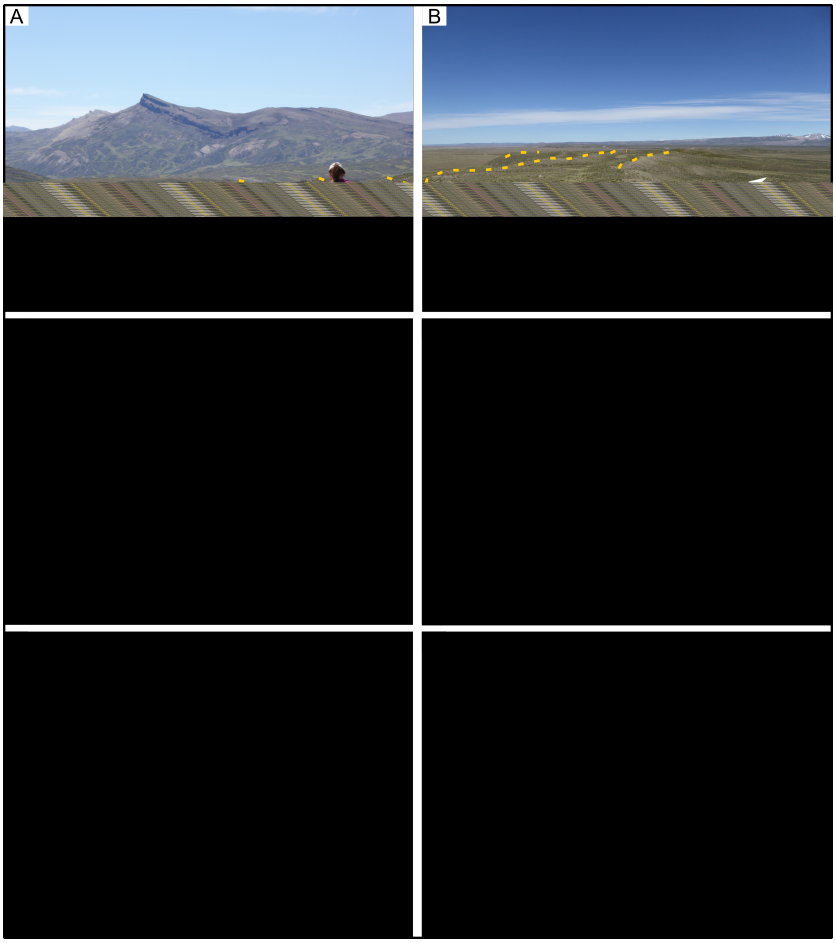

Figure 4: A) Photograph showing the Menelik moraines (dashed yellow lines) draped on higher ground. B-E) Photographs showing the outermost Menelik moraines (dashed yellow lines) along with examples of sampled boulders. F) Example of a cobble sampled from the outwash associated with Menelik moraines. Ventifacts on the surface suggest long surface exposure (cf. Hein et al., 2011).

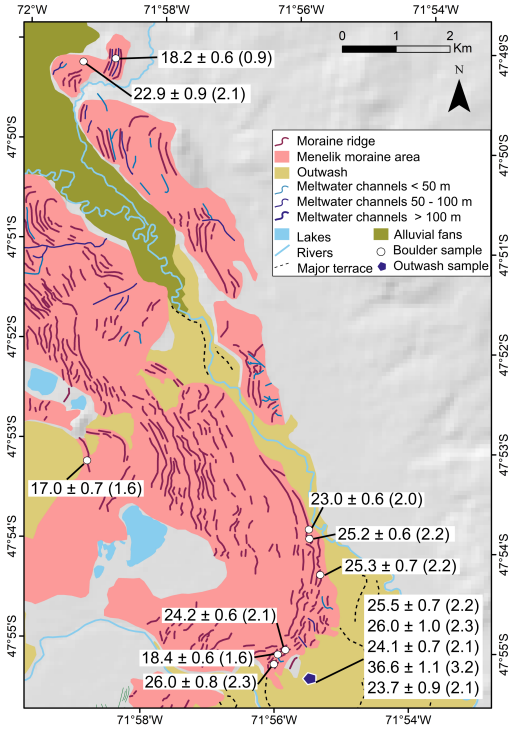

Figure 5: Enlarged geomorphological map showing the Menelik moraine system along with sample locations and ^{10}Be exposure ages.

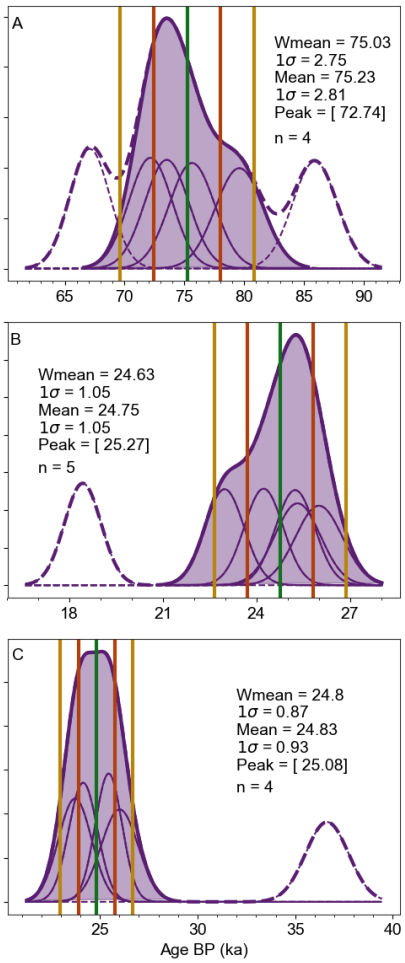

Figure 6: Probability density diagrams ('camelplots') for A) the Klementek cobble ages, A) Menelik boulder ages, and C) Menelik cobble ages. Thin purple curves represent Gaussian curves for individual samples. Thick purple curve represent the summed probability distribution for the data, excluding outliers. Outliers are represented by dashed curves. Vertical lines denote an arithmetic mean (dark green, excluding outliers), and 1 and 2 σ (paired brown and yellow lines respectively) confidence intervals of the mean. Wmean: uncertainty-weighted mean.

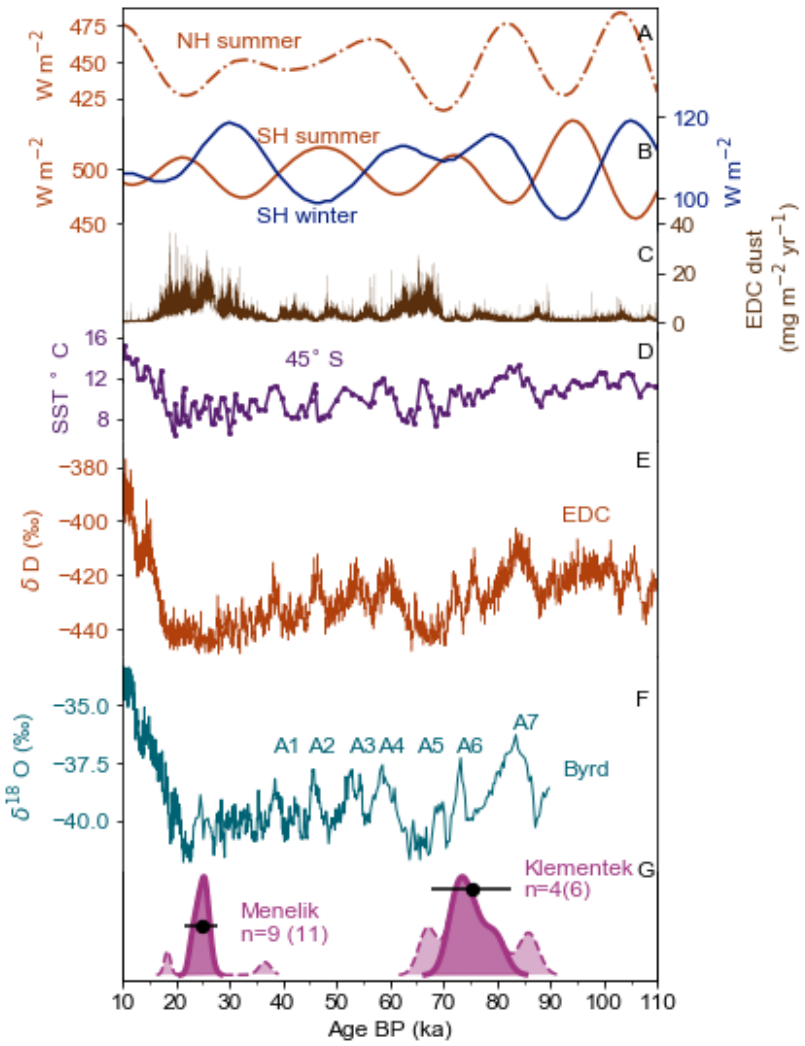
NH summer
SH summer
SH winter
W m−2
475
450
425
500
450
A
B
C
120
100
40
20
0
EDC dust
(mg m−2 yr−1)
45° S
SST ° C
16
12
8
D
E
EDC
δ D (‰)
−380
−400
−420
−440
F
δ18 O (‰)
−35.0
−37.5
−40.0
A1 A2 A3 A4 A5 A6 A7
Byrd
Klementek
n=4(6)
G
Menelik
n=9 (11)
10 20 30 40 50 60 70 80 90 100 110
Age BP (ka)

Figure 7

Figure 7: Comparison of our ^{10}Be ages and other proxies. A: July insolation intensity for 60° N (Berger and Loutre, 1991). B: July (orange) and December (blue) insolation intensity for 50° S (Berger and Loutre, 1991). C: EDC dust record (Lambert et al., 2012). D: SST (Mg/CA) record from off New Zealand (MD97-2120) (Pahnke et al., 2003). E: EDC deuterium record (EPICA Community Members, 2004) plotted on AICC2012 timescale (Veres et al., 2013). F: Oxygen isotope record from Byrd ice core (Johnsen et al., 1972) plotted on GISP2 timescale (Blunier, 2001). G: Summed probability density functions ('camelplots') for the Klementek outwash, and the Menelik boulders and outwash cobbles combined (plotted on individual y-axis; dashed curves represent outliers). Circles indicate the arithmetic means of the Klementek and Menelik ages (after outliers have been excluded) and error bars indicate uncertainty of the mean, which includes propagated individual internal uncertainties of the ^{10}Be ages and production rate uncertainty (Kaplan et al., 2011).

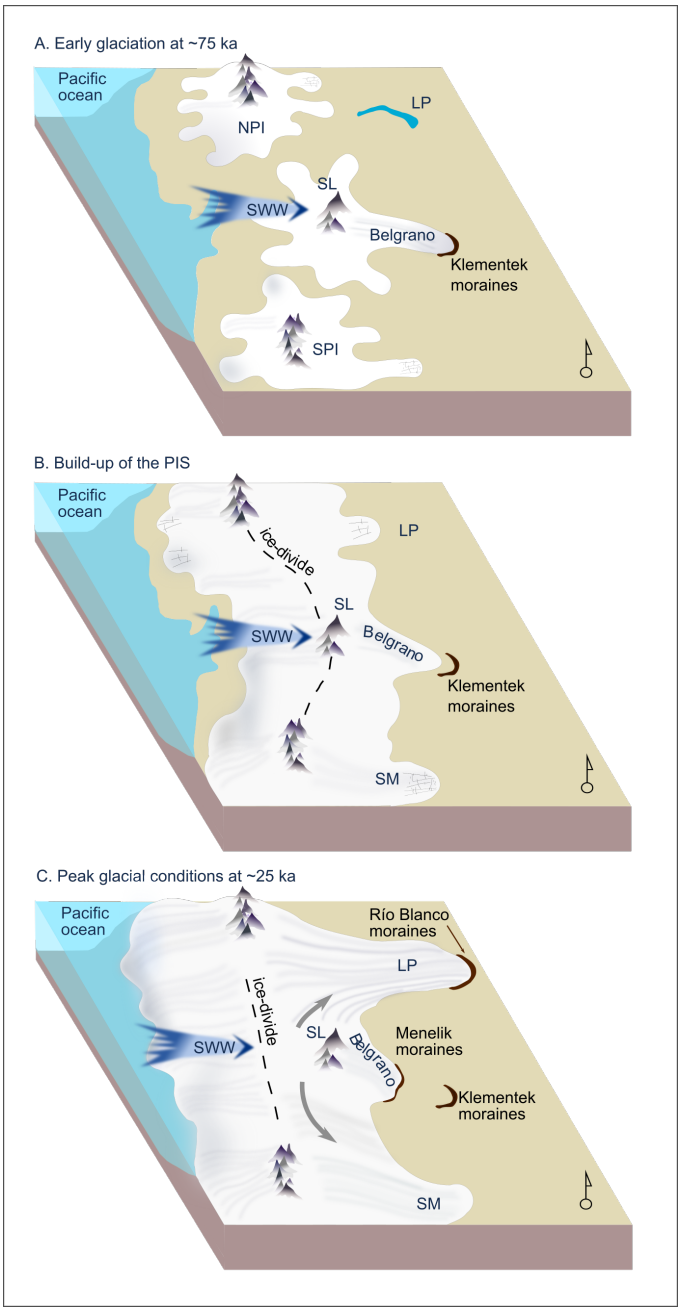
A. Early glaciation at ~75 ka
Pacific ocean
NPI
LP
SL
SWW
Belgrano
Klementek moraines
SPI
B. Build-up of the PIS
Pacific ocean
ice-divide
LP
SL
SWW
Belgrano
Klementek moraines
SM
C. Peak glacial conditions at ~25 ka
Pacific ocean
Río Blanco moraines
LP
ice-divide
SL
SWW
Belgrano
Menelik moraines
Klementek moraines
SM

Figure 8

Figure 8: A conceptual model of the build-up of the last Patagonian Ice Sheet (PIS). A) The initial inception of the Patagonian Ice Sheet begins with nucleation centres over the present day North and South Patagonian Icefields (NPI, SPI), and the San Lorenzo massif (SL), likely triggered by reduced summer insolation in the southern hemisphere. At this time, the Southern Westerly Winds (SWW) can freely penetrate through the topographic depression between the present icefields to bring snowfall east to the San Lorenzo ice cap. Ice expansion is greatest down the high-elevation eastern Belgrano valley, since glaciers draining to the south, west and north of the massif descended into deep valleys. B) The individual ice masses coalesce, causing reorganization of ice (and fluvial) drainage routes, and reducing ice flux down the Belgrano valley. C) Under peak glacial conditions, the ice-divide increased in elevation, and migrated westward towards the precipitation source. This caused snow starvation to the San Lorenzo massif, and significant re-organization of ice-drainage routes to focus ice flow into the major outlets of the Patagonian Ice Sheet that surround the San Lorenzo massif (LP and SM). These processes limited ice expansion in the Belgrano valley when the major outlet to its north, LP (and also LBA, which is not shown) was near its maximum last glacial extent indicated by the Río Blanco moraines (Hein et al., 2010).

References

Abramowski, U., Bergau, A., Seebach, D., Zech, R., Glaser, B., Sosin, P., Kubik, P.W., Zech, W., 2006. Pleistocene glaciations of Central Asia: results from 10Be surface exposure ages of erratic boulders from the Pamir (Tajikistan), and the Alay-Turkestan range (Kyrgyzstan). Quaternary Science Reviews 25, 1080–1096.

Applegate, P.J., Urban, N.M., Laabs, B.J., Keller, K., Alley, R.B., 2010. Modeling the statistical distributions of cosmogenic exposure dates from moraines. Geoscientific Model Development 3, 293–307.

Balco, G., Stone, J.O., Lifton, N.A., Dunai, T.J., 2008. A complete and easily accessible means of calculating surface exposure ages or erosion rates from 10Be and 26Al measurements. Quaternary Geochronology 3, 174–195.

Barrows, T.T., Juggins, S., De Deckker, P., Calvo, E., Pelejero, C., 2007. Long-term sea surface temperature and climate change in the Australian-New Zealand region. Paleoceanography 22, 1–17.

Bendle, J.M., Palmer, A.P., Thorndycraft, V.R., Matthews, I.P., 2017a. High-resolution chronology for deglaciation of the Patagonian Ice Sheet at Lago Buenos Aires (46.5°S) revealed through varve chronology and Bayesian age modelling. Quaternary Science Reviews 177, 314–339.

Bendle, J.M., Thorndycraft, V.R., Palmer, A.P., 2017b. The glacial geomorphology of the Lago Buenos Aires and Lago Pueyrredón ice lobes of central Patagonia. Journal of Maps 13, 654–673.

Berger, A., Loutre, M.F., 1991. Insolation values for the climate of the last 10 million years. Quaternary Science Reviews 10, 297–317.

Bierman, P.R., Caffee, M.W., Davis, P.T., Marsella, K., Pavich, M., Colgan, P., Mickelson, D., Larsen, J., 2002. Rates and Timing of Earth Surface Processes From In Situ-Produced Cosmogenic Be-10. Reviews in Mineralogy and Geochemistry 50, 147–205.

Blunier, T., 2001. Timing of Millennial-Scale Climate Change in Antarctica and Greenland During the Last Glacial Period. Science 291, 109–112.

Boex, J., Fogwill, C., Harrison, S., Glasser, N.F., Hein, A., Schnabel, C., Xu, S., 2013. Rapid thinning of the late Pleistocene Patagonian Ice Sheet followed migration of the Southern Westerlies. Scientific Reports 3, 2118.

Borchers, B., Marrero, S., Balco, G., Caffee, M., Goehring, B., Lifton, N., Nishiizumi, K., Phillips, F., Schaefer, J., Stone, J., 2016. Geological calibration of spallation production rates in the CRONUS-Earth project. Quaternary Geochronology 31, 188–198.

Briner, J.P., Kaufman, D.S., Manley, W.F., Finkel, R.C., Caffee, M.W., 2005. Cosmogenic exposure dating of late Pleistocene moraine stabilization in Alaska. Bulletin of the Geological Society of America 117, 1108–1120.

Bronk Ramsey, C., 2009. Bayesian Analysis of Radiocarbon Dates. Radiocarbon 51, 337–360.

Buizert, C., Sigl, M., Severi, M., Markle, B.R., Wettstein, J.J., McConnell, J.R., Pedro, J.B., Sodemann, H., Goto-Azuma, K., Kawamura, K., Fujita,

S., Motoyama, H., Hirabayashi, M., Uemura, R., Stenni, B., Parrenin, F., He, F., Fudge, T.J., Steig, E.J., 2018. Abrupt ice-age shifts in southern westerly winds and Antarctic climate forced from the north. Nature 563, 681–685.

Caldenius, C., 1932. Las glaciaciones cuaternarias en la Patagonia y Tierra del Fuego. Geografiska Annaler 14, 1–164.

Caniupán, M., Lamy, F., Lange, C.B., Kaiser, J., Arz, H., Kilian, R., Baeza Urrea, O., Aracena, C., Hebbeln, D., Kissel, C., Laj, C., Mollenhauer, G., Tiedemann, R., 2011. Millennial-scale sea surface temperature and Patagonian Ice Sheet changes off southernmost Chile (53 °S) over the past 60 kyr. Paleoceanography 26, 1–10.

Clark, P.U., Dyke, A.S., Shakun, J.D., Carlson, A.E., Clark, J., Wohlfarth, B., Mitrovica, J.X., Hostetler, S.W., McCabe, A.M., 2009. The Last Glacial Maximum. Science 325, 710–714.

Cogez, A., Herman, F., Pelt, E., Reuschlé, T., Morvan, G., Darvill, C.M., Norton, K.P., Christl, M., Märki, L., Chabaux, F., 2018. U-Th and 10Be constraints on sediment recycling in proglacial settings, Lago Buenos Aires, Patagonia. Earth Surface Dynamics 6, 121–140.

Darvill, C.M., 2013. Cosmogenic nuclide analysis. Geomophological techniques 10, 1–25.

Darvill, C.M., Bentley, M.J., Stokes, C.R., Hein, A.S., Rodes, À., 2015. Extensive MIS 3 glaciation in southernmost Patagonia revealed by cosmo-

genic nuclide dating of outwash sediments. Earth and Planetary Science Letters 429, 157–169.

Darvill, C.M., Bentley, M.J., Stokes, C.R., Shulmeister, J., 2016. The timing and cause of glacial advances in the southern midlatitudes during the last glacial cycle based on a synthesis of exposure ages from Patagonia and New Zealand. Quaternary Science Reviews 149, 200–214.

Darvill, C.M., Stokes, C.R., Bentley, M.J., Lovell, H., 2014. A glacial geomorphological map of the southernmost ice lobes of Patagonia: the Bahía Inútil – San Sebastián, Magellan, Otway, Skyring and Río Gallegos lobes. Journal of Maps 10, 500–520.

Davies, B., Thorndycraft, V., Fabel, D., Martin, J., 2018. Asynchronous glacier dynamics during the Antarctic Cold Reversal in central Patagonia. Quaternary Science Reviews 200, 287–312.

De Angelis, H., Miles, E., Moelg, N., Paul, F., Sharp, M., Wyatt, F., 2015. GLIMS Glacier Database.

Denton, G., Heusser, C.J., Lowel, T., Moreno, P., Andersen, B., Heusser, L.E., Schluhter, C., Marchant, D., 1999a. Interhemispheric Linkage of Paleoclimate During the Last Glaciation. Geografiska Annaler, Series A: Physical Geography 81, 107–153.

Denton, G.H., Lowell, T.V., Heusser, C.J., Schluchter, C., Andersen, B.G., Heusser, L.E., Moreno, P.I., Marchant, D.R., 1999b. Geomorphology, stratigraphy, and radiocarbon chronology of Llanquihue Drift in the area

of the Southern Lake District, Seno Reloncavi, and Isla Grande de Chiloe, Chile. Geografiska Annaler Series A Physical Geography 81 A, 167–229.

Dong, G., Zhou, W., Yi, C., Fu, Y., Zhang, L., Li, M., 2018. The timing and cause of glacial activity during the last glacial in central Tibet based on 10Be surface exposure dating east of Mount Jaggang, the Xainza range. Quaternary Science Reviews 186, 284–297.

Doughty, A.M., Schaefer, J.M., Putnam, A.E., Denton, G.H., Kaplan, M.R., Barrell, D.J.A., Andersen, B.G., Kelley, S.E., Finkel, R.C., Schwartz, R., 2015. Mismatch of glacier extent and summer insolation in Southern Hemisphere mid-latitudes. Geology 43, 407–410.

Douglass, D.C., Bockheim, J.G., 2006. Soil-forming rates and processes on Quaternary moraines near Lago Buenos Aires, Argentina. Quaternary Research 65, 293–307.

EPICA Community Members, 2004. Eight glacial cycles from an Antarctic ice core. Nature 429, 623–628.

EPICA Community Members, 2006. One-to-one coupling of glacial climate variability in Greenland and Antarctica. Nature 444, 195–198.

Falaschi, D., Bolch, T., Rastner, P., Lenzano, M.G., Lenzano, L., Lo Vecchio, A., Moragues, S., 2017. Mass changes of alpine glaciers at the eastern margin of the Northern and Southern Patagonian Icefields between 2000 and 2012. Journal of Glaciology 63, 258–272.

Falaschi, D., Bravo, C., Masiokas, M., Villalba, R., Rivera, A., 2013. First Glacier Inventory and Recent Changes in Glacier Area in the Monte San

Lorenzo Region (47°S), Southern Patagonian Andes, South America. Arctic, Antarctic, and Alpine Research 45, 19–28.

Farquharson, L., Mann, D., Rittenour, T., Groves, P., Grosse, G., Jones, B., 2018. Alaskan marine transgressions record out-of-phase Arctic Ocean glaciation during the last interglacial. Geology 46, 783–786.

Finkel, R.C., Owen, L.A., Barnard, P.L., Caffee, M.W., 2003. Beryllium-10 dating of Mount Everest moraines indicates a strong monsoon influence and glacial synchroneity throughout the Himalaya. Geology 31, 561.

García, J.L., Hall, B.L., Kaplan, M.R., Vega, R.M., Strelin, J.A., 2014. Glacial geomorphology of the Torres del Paine region (southern Patagonia): Implications for glaciation, deglaciation and paleolake history. Geomorphology 204, 599–616.

García, J.L., Hein, A.S., Binnie, S.A., Gómez, G.A., González, M.A., Dunai, T.J., 2018. The MIS 3 maximum of the Torres del Paine and Última Esperanza ice lobes in Patagonia and the pacing of southern mountain glaciation. Quaternary Science Reviews 185, 9–26.

García, J.L., Maldonado, A., de Porras, M.E., Nuevo Delaunay, A., Reyes, O., Ebensperger, C.A., Binnie, S.A., Lüthgens, C., Méndez, C., 2019. Early deglaciation and paleolake history of Río Cisnes Glacier, Patagonian Ice Sheet (44°S). Quaternary Research 91, 194–217.

Garreaud, R., Lopez, P., Minvielle, M., Rojas, M., 2013. Large-scale control on the Patagonian climate. Journal of Climate 26, 215–230.

Garreaud, R.D., Vuille, M., Compagnucci, R., Marengo, J., 2009. Present-day South American climate. Palaeogeography, Palaeoclimatology, Palaeoecology 281, 180–195.

Gillespie, A., Molnar, P., 1995. Asynchronous maximum advances of mountain and continental glaciers. Reviews of Geophysics 33, 311–364.

Gillespie, A.R., Bierman, P.R., 1995. Precision of terrestrial exposure ages and erosion rates estimated from analysis of cosmogenic isotopes produced in situ. Journal of Geophysical Research: Solid Earth 100, 24637–24649.

Glasser, N.F., Harrison, S., Schnabel, C., Fabel, D., Jansson, K.N., 2012. Younger Dryas and early Holocene age glacier advances in Patagonia. Quaternary Science Reviews 58, 7–17.

Glasser, N.F., Jansson, K.N., Goodfellow, B.W., de Angelis, H., Rodnight, H., Rood, D.H., 2011. Cosmogenic nuclide exposure ages for moraines in the Lago San Martin Valley, Argentina. Quaternary Research 75, 636–646.

Glasser, N.F., Jansson, K.N., Harrison, S., Kleman, J., 2008. The glacial geomorphology and Pleistocene history of South America between 38°S and 56°S. Quaternary Science Reviews 27, 365–390.

Gosse, J.C., Phillips, F.M., 2001. Terrestrial in situ cosmogenic nuclides: Theory and application. Quaternary Science Reviews 20, 1475–1560.

Hallet, B., Putkonen, J., 1994. Surface dating of dynamic landforms: Young boulders on aging moraines. Science 265, 937–940.

Hays, J.D., Imbrie, J., Shackleton, N.J., 1976. Variations in the Earth's Orbit: Pacemaker of the Ice Ages. Science 194, 1121–1132.

Hein, A.S., 2009. Quaternary Glaciations in the Lago Pueyrredon Valley, Argentina. Ph.D. thesis. The University of Edinburgh.

Hein, A.S., Cogez, A., Darvill, C.M., Mendelova, M., Kaplan, M.R., Herman, F., Dunai, T.J., Norton, K., Xu, S., Christl, M., Rodés, Á., 2017. Regional mid-Pleistocene glaciation in central Patagonia. Quaternary Science Reviews 164, 77–94.

Hein, A.S., Dunai, T.J., Hulton, N.R.J., Xu, S., 2011. Exposure dating outwash gravels to determine the age of the greatest Patagonian glaciations. Geology 39, 103–106.

Hein, A.S., Hulton, N.R., Dunai, T.J., Schnabel, C., Kaplan, M.R., Naylor, M., Xu, S., 2009. Middle Pleistocene glaciation in Patagonia dated by cosmogenic-nuclide measurements on outwash gravels. Earth and Planetary Science Letters 286, 184–197.

Hein, A.S., Hulton, N.R., Dunai, T.J., Sugden, D.E., Kaplan, M.R., Xu, S., 2010. The chronology of the Last Glacial Maximum and deglacial events in central Argentine Patagonia. Quaternary Science Reviews 29, 1212–1227.

Henríquez, W.I., Villa-Martínez, R., Vilanova, I., De Pol-Holz, R., Moreno, P.I., 2017. The last glacial termination on the eastern flank of the central Patagonian Andes (47 ° S). Climate of the Past 13, 879–895.

Herber, L., 1969. Separation of feldspar from quartz by flotation. The American Mineralogist 54, 1212–1215.

Heusser, L., Heusser, C., Kleczkowski, A., Crowhurst, S., 1999. A 50,000-yr Pollen Record from Chile of South American Millennial-Scale Climate Instability during the Last Glaciation. Quaternary Research 52, 154–158.

Heyman, J., Applegate, P.J., Blomdin, R., Gribenski, N., Harbor, J.M., Stroeven, A.P., 2016. Boulder height – exposure age relationships from a global glacial 10Be compilation. Quaternary G 34, 1–11.

Heyman, J., Stroeven, A.P., Harbor, J.M., Caffee, M.W., 2011. Too young or too old: Evaluating cosmogenic exposure dating based on an analysis of compiled boulder exposure ages. Earth and Planetary Science Letters 302, 71–80.

Hogg, A.G., Hua, Q., Blackwell, P.G., Niu, M., Buck, C.E., Guilderson, T.P., Heaton, T.J., Palmer, J.G., Reimer, P.J., Reimer, R.W., Turney, C.S.M., Zimmerman, S.R.H., 2013. SHCal13 Southern Hemisphere Calibration, 0–50,000 Years cal BP. Radiocarbon 55, 1889–1903.

Horta, L.R., Georgieff, S.M., Aschero, C.A., Goñi, R.A., 2017. Paleolacustrine records from Late Pleistocene – Holocene in the Perito Moreno National Park, Argentinian Patagonian Andes. Quaternary International 436, 8–15.

Hughes, P.D., Gibbard, P.L., 2018. Global glacier dynamics during 100 ka Pleistocene glacial cycles. Quaternary Research 90, 222–243.

Hughes, P.D., Gibbard, P.L., Ehlers, J.J., 2013. Timing of glaciation during the last glacial cycle: Evaluating the concept of a global 'Last Glacial Maximum' (LGM). Earth-Science Reviews 125, 171–198.

Johnsen, S.J., Dansgaard, W., Clausen, H.B., Langway, C.C., 1972. Oxygen isotope profiles through the antarctic and greenland ice sheets. Nature 235, 429–434.

Kaiser, J., Lamy, F., 2010. Links between Patagonian Ice Sheet fluctuations and Antarctic dust variability during the last glacial period (MIS 4-2). Quaternary Science Reviews 29, 1464–1471.

Kaiser, J., Lamy, F., Hebbeln, D., 2005. A 70-kyr sea surface temperature record off southern Chile (Ocean Drilling Program Site 1233). Paleoceanography 20, PA4009.

Kaplan, M., Moreno, P., Rojas, M., 2008. Glacial dynamics in southernmost South America during Marine Isotope Stage 5e to the Younger Dryas chron: a brief review with a focus on cosmogenic nuclide measurements. Journal of Quaternary Science 23, 649–658.

Kaplan, M.R., Ackert, R.P., Singer, B.S., Douglass, D.C., Kurz, M.D., 2004. Cosmogenic nuclide chronology of millennial-scale glacial advances during O-isotope stage 2 in Patagonia. Bulletin of the Geological Society of America 116, 308–321.

Kaplan, M.R., Douglass, D.C., Singer, B.S., Ackert, R.P., Caffee, M.W., 2005. Cosmogenic nuclide chronology of pre-last glacial maximum moraines at Lago Buenos Aires, 46°S, Argentina. Quaternary Research 63, 301–315.

Kaplan, M.R., Strelin, J.A., Schaefer, J.M., Denton, G.H., Finkel, R.C., Schwartz, R., Putnam, A.E., Vandergoes, M.J., Goehring, B.M., Travis, S.G., 2011. In-situ cosmogenic 10Be production rate at Lago Argentino,

Patagonia: Implications for late-glacial climate chronology. Earth and Planetary Science Letters 309, 21–32.

Kelley, S.E., Kaplan, M.R., Schaefer, J.M., Andersen, B.G., Barrell, D.J.A., Putnam, A.E., Denton, G.H., Schwartz, R., Finkel, R.C., Doughty, A.M., 2014. High-precision 10 Be chronology of moraines in the Southern Alps indicates synchronous cooling in Antarctica and New Zealand 42,000 years ago. Earth and Planetary Science Letters 405, 194–206.

Kilian, R., Lamy, F., 2012. A review of Glacial and Holocene paleoclimate records from southernmost Patagonia (49–55°S). Quaternary Science Reviews 53, 1–23.

Koppes, M., Gillespie, A.R., Burke, R.M., Thompson, S.C., Stone, J., 2008. Late Quaternary glaciation in the Kyrgyz Tien Shan. Quaternary Science Reviews 27, 846–866.

Lagabrielle, Y., Suárez, M., Rossello, E.A., Hérail, G., Martinod, J., Régnier, M., de la Cruz, R., 2004. Neogene to Quaternary tectonic evolution of the Patagonian Andes at the latitude of the Chile Triple Junction. Tectonophysics 385, 211–241.

Lal, D., 1991. Cosmic ray labeling of erosion surfaces: in situ nuclide production rates and erosion models. Earth and Planetary Science Letters 104, 424–439.

Lambert, F., Bigler, M., Steffensen, J.P., Hutterli, M.A., Fischer, H., 2012. EDC dust flux 800 kyr (full resolution).

Lambert, F., Delmonte, B., Petit, J.R., Bigler, M., Kaufmann, P.R., Hutterli, M.A., Stocker, T.F., Ruth, U., Steffensen, J.P., Maggi, V., 2008. Dust-climate couplings over the past 800,000 years from the EPICA Dome C ice core. Nature 452, 616–619.

Lamy, F., 2004. Antarctic Timing of Surface Water Changes off Chile and Patagonian Ice Sheet Response. Science 304, 1959–1962.

Lamy, F., Arz, H.W., Kilian, R., Lange, C.B., Lembke-Jene, L., Wengler, M., Kaiser, J., Baeza-Urrea, O., Hall, I.R., Harada, N., Tiedemann, R., 2015. Glacial reduction and millennial-scale variations in Drake Passage throughflow. Proceedings of the National Academy of Sciences 112, 13496–13501.

Lewis, C.J., McDonald, E.V., Sancho, C., Peña, J.L., Rhodes, E.J., 2009. Climatic implications of correlated Upper Pleistocene glacial and fluvial deposits on the Cinca and Gállego Rivers (NE Spain) based on OSL dating and soil stratigraphy. Global and Planetary Change 67, 141–152.

Markgraf, V., Whitlock, C., Haberle, S., 2007. Vegetation and fire history during the last 18,000 cal yr B.P. in Southern Patagonia: Mallín Pollux, Coyhaique, Province Aisén (45°41'30" S, 71°50'30" W, 640 m elevation). Palaeogeography, Palaeoclimatology, Palaeoecology 254, 492–507.

Markle, B.R., Steig, E.J., Buizert, C., Schoenemann, S.W., Bitz, C.M., Fudge, T.J., Pedro, J.B., Ding, Q., Jones, T.R., White, J.W., Sowers, T., 2017. Global atmospheric teleconnections during Dansgaard-Oeschger events. Nature Geoscience 10, 36–40.

Martin, J.R., Davies, B.J., Thorndycraft, V.R., 2019. Glacier dynamics during a phase of Late Quaternary warming in Patagonia reconstructed from sediment-landform associations. Geomorphology 337, 111–133.

Martínez-Garcia, A., Rosell-Melé, A., Jaccard, S.L., Geibert, W., Sigman, D.M., Haug, G.H., 2011. Southern Ocean dust–climate coupling over the past four million years. Nature 476, 312–315.

McCarthy, A., Mackintosh, A., Rieser, U., Fink, D., 2008. Mountain Glacier Chronology from Boulder Lake, New Zealand, Indicates MIS 4 and MIS 2 Ice Advances of Similar Extent. Arctic, Antarctic, and Alpine Research 40, 695–708.

McCulloch, R.D., Fogwill, C.J., Sugden, D.E., Bentley, M.J., Kubik, P.W., 2005. Chronology of the Last Glaciation in Central Strait of Magellan and Bahía Inútil, Southernmost South America. Geografiska Annaler, Series A: Physical Geography 87, 289–312.

Mendelova, M., Hein, A., McCulloch, R., Davies, B., 2017. The Last Glacial Maximum and deglaciation in central Patagonia, 44°S–49°S. Cuadernos de Investigación Geográfica 43, 719.

Mercer, J.H., 1968. Variations of some Patagonian glaciers since the Late-Glacial. American Journal of Science 266, 91–109.

Mercer, J.H., 1976. Glacial history of southernmost South America. Quaternary Research 6, 125–166.

Mercer, J.H., 1984. Simultaneous climatic change in both hemispheres and similar bipolar interglacial warming: Evidence and implications, in:

Hansen, J.E., Takahashi, T. (Eds.), Climate Processes and Climate Sensitivity. American Geophysical Union, Washington, D. C.. volume 29 of *Geophysical Monograph Series*, pp. 307–313.

Milankovitch, M., 1941. Kanon der Erdbestrahlung und Seine Andwendung auf das Eiszeitenproblem. Belgrade.

Moreno, P.I., Denton, G.H., Moreno, H., Lowell, T.V., Putnam, A.E., Kaplan, M.R., 2015. Radiocarbon chronology of the last glacial maximum and its termination in northwestern Patagonia. Quaternary Science Reviews 122, 233–249.

Murdie, R.E., Pugh, D.T., Styles, P., 1998. A lightweight, portable, digital probe for measuring the thermal gradient in shallow water sediments, with examples from Patagonia. Geo-Marine Letters 18, 315–320.

Nishiizumi, K., Imamura, M., Caffee, M.W., Southon, J.R., Finkel, R.C., McAninch, J., 2007. Absolute calibration of 10Be AMS standards. Nuclear Instruments and Methods in Physics Research, Section B: Beam Interactions with Materials and Atoms 258, 403–413.

Owen, L.A., Finkel, R.C., Caffee, M.W., 2002. A note on the extent of glaciation throughout the Himalaya during the global Last Glacial Maximum. Quaternary Science Reviews 21, 147–157.

Owen, L.A., Finkel, R.C., Haizhou, M., Spencer, J.Q., Derbyshire, E., Barnard, P.L., Caffee, M.W., 2003. Timing and style of Late Quaternary glaciation in northeastern Tibet. Bulletin of the Geological Society of America 115, 1356–1364.

Pahnke, K., Zahn, R., Elderfield, H., Schulz, M., 2003. 340,000-Year Centennial-Scale Marine Record of Southern Hemisphere Climatic Oscillation. Science 301, 948–952.

Pallàs, R., Rodés, Á., Braucher, R., Bourlès, D., Delmas, M., Calvet, M., Gunnell, Y., 2010. Small, isolated glacial catchments as priority targets for cosmogenic surface exposure dating of Pleistocene climate fluctuations, southeastern Pyrenees. Geology 38, 891–894.

Pedro, J.B., Jochum, M., Buizert, C., He, F., Barker, S., Rasmussen, S.O., 2018. Beyond the bipolar seesaw: Toward a process understanding of interhemispheric coupling. Quaternary Science Reviews 192, 27–46.

Porter, S.C., Swanson, T.W., 2008. 36Cl dating of the classic pleistocene glacial record in the northeastern Cascade Range, Washington. American Journal of Science 308, 130–166.

Putkonen, J., Swanson, T., 2003. Accuracy of cosmogenic ages for moraines. Quaternary Research 59, 255–261.

Putnam, A.E., Schaefer, J.M., Barrell, D.J.A., Vandergoes, M., Denton, G.H., Kaplan, M.R., Finkel, R.C., Schwartz, R., Goehring, B.M., Kelley, S.E., 2010. In situ cosmogenic 10Be production-rate calibration from the Southern Alps, New Zealand. Quaternary Geochronology 5, 392–409.

Putnam, A.E., Schaefer, J.M., Denton, G.H., Barrell, D.J., Birkel, S.D., Andersen, B.G., Kaplan, M.R., Finkel, R.C., Schwartz, R., Doughty, A.M., 2013. The Last Glacial Maximum at 44°S documented by a 10Be moraine

chronology at Lake Ohau, Southern Alps of New Zealand. Quaternary Science Reviews 62, 114–141.

Ramos, V.A., Kay, S.M., 1992. Southern Patagonian plateau basalts and deformation: Backarc testimony of ridge collisions. Tectonophysics 205, 261–282.

Ramos, V.A., Niemeyer, H., Skarmeta, J., Muñoz, J., 1982. Magmatic evolution of the Austral Patagonian Andes. Earth Science Reviews 18, 411–443.

Röhringer, I., Zech, R., Abramowski, U., Sosin, P., Aldahan, A., Kubik, P.W., Zöller, L., Zech, W., 2012. The late Pleistocene glaciation in the Bogchigir Valleys (Pamir, Tajikistan) based on 10 Be surface exposure dating. Quaternary Research 78, 590–597.

Sagredo, E., Lowell, T., 2012. Climatology of Andean glaciers: A framework to understand glacier response to climate change. Global and Planetary Change 86-87, 101–109.

Sagredo, E., Moreno, P., Villa-Martínez, R., Kaplan, M., Kubik, P., Stern, C., 2011. Fluctuations of the Última Esperanza ice lobe (52°S), Chilean Patagonia, during the last glacial maximum and termination 1. Geomorphology 125, 92–108.

Sagredo, E.A., Kaplan, M.R., Araya, P.S., Lowell, T.V., Aravena, J.C., Moreno, P.I., Kelly, M.A., Schaefer, J.M., 2018. Trans-pacific glacial response to the Antarctic Cold Reversal in the southern mid-latitudes. Quaternary Science Reviews 188, 160–166.

Sagredo, E.A., Lowell, T.V., Kelly, M.A., Rupper, S., Aravena, J.C., Ward, D.J., Malone, A.G., 2017. Equilibrium line altitudes along the Andes during the Last millennium: Paleoclimatic implications. The Holocene 27, 1019–1033.

Schaefer, J.M., Putnam, A.E., Denton, G.H., Kaplan, M.R., Birkel, S., Doughty, A.M., Kelley, S., Barrell, D.J.A., Finkel, R.C., Winckler, G., Anderson, R.F., Ninneman, U.S., Barker, S., Schwartz, R., Andersen, B.G., Schluechter, C., 2015. The Southern Glacial Maximum 65,000 years ago and its Unfinished Termination. Quaternary Science Reviews 114, 52–60.

Shulmeister, J., 1999. Australasian evidence for mid-Holocene climate change implies precessional control of Walker Circulation in the Pacific. Quaternary International 57-58, 81–91.

Shulmeister, J., Goodwin, I., Renwick, J., Harle, K., Armand, L., McGlone, M., Cook, E., Dodson, J., Hesse, P., Mayewski, P., Curran, M., 2004. The Southern Hemisphere westerlies in the Australasian sector over the last glacial cycle: a synthesis. Quaternary International 118-119, 23–53.

Shulmeister, J., Thackray, G.D., Rieser, U., Hyatt, O.M., Rother, H., Smart, C.C., Evans, D.J., 2010. The stratigraphy, timing and climatic implications of glaciolacustrine deposits in the middle Rakaia Valley, South Island, New Zealand. Quaternary Science Reviews 29, 2362–2381.

Shulmeister, J., Thackray, G.D., Rittenour, T.M., Fink, D., Patton, N.R., 2019. The timing and nature of the last glacial cycle in New Zealand. Quaternary Science Reviews 206, 1–20.

Shulmeister, J., Thackray, G.D., Rittenour, T.M., Hyatt, O.M., 2018. Multiple glacial advances in the Rangitata Valley, South Island, New Zealand, imply roles for Southern Hemisphere westerlies and summer insolation in MIS 3 glacial advances. Quaternary Research 89, 375–393.

Singer, B.S., Ackert, R.P., Guillou, H., 2004. 40Ar/39Ar and K-Ar chronology of Pleistocene glaciations in Patagonia. Geological Society of America Bulletin 116, 434.

Smedley, R.K., Glasser, N.F., Duller, G.A.T., 2016. Luminescence dating of glacial advances at Lago Buenos Aires (˜46°S), Patagonia. Quaternary Science Reviews 134, 59–73.

Stocker, T.F., Johnsen, S.J., 2003. A minimum thermodynamic model for the bipolar seesaw. Paleoceanography 18, 1–9.

Stone, J.O., 2000. Air pressure and cosmogenic isotope production. Journal of Geophysical Research: Solid Earth 105, 23753–23759.

Sugden, D., Bentley, M., Fogwill, C., Hulton, N., Mcculloch, R., Purves, R., 2005. Late-glacial glacier events in southernmost south america: a blend of 'northern' and 'southern' hemispheric climatic signals? Geografiska Annaler: Series A, Physical Geography 87, 273–288.

Sugden, D.E., Hulton, N.R.J., Purves, R.S., 2002. Modelling the inception of the Patagonian icesheet. Quaternary International 95-96, 55–64.

Sugden, D.E., McCulloch, R.D., Bory, A.J.M., Hein, A.S., 2009. Influence of Patagonian glaciers on Antarctic dust deposition during the last glacial period. Nature Geoscience 2, 281–285.

Sutherland, R., Kim, K., Zondervan, A., McSaveney, M., 2007. Orbital forcing of mid-latitude Southern Hemisphere glaciation since 100 ka inferred from cosmogenic nuclide ages of moraine boulders from the Cascade Plateau, southwest New Zealand. Bulletin of the Geological Society of America 119, 443–451.

Svendsen, J.I., Alexanderson, H., Astakhov, V.I., Demidov, I., Dowdeswell, J.A., Funder, S., Gataullin, V., Henriksen, M., Hjort, C., Houmark-Nielsen, M., Hubberten, H.W., Ingólfsson, Ó., Jakobsson, M., Kjær, K.H., Larsen, E., Lokrantz, H., Lunkka, J.P., Lysså, A., Mangerud, J., Matiouchkov, A., Murray, A., Möller, P., Niessen, F., Nikolskaya, O., Polyak, L., Saarnisto, M., Siegert, C., Siegert, M.J., Spielhagen, R.F., Stein, R., 2004. Late Quaternary ice sheet history of northern Eurasia. Quaternary Science Reviews 23, 1229–1271.

Thackray, G.D., 2001. Extensive early and middle Wisconsin Glaciation on the western Olympic Peninsula, Washington, and the variability of Pacific moisture delivery to the northwestern United States. Quaternary Research 55, 257–270.

Vandergoes, M.J., Newnham, R.M., Preusser, F., Hendy, C.H., Lowell, T.V., Fitzsimons, S.J., Hogg, A.G., Kasper, H.U., Schlüchter, C., 2005. Regional insolation forcing of late Quaternary climate change in the Southern Hemisphere. Nature 436, 242–245.

Veres, D., Bazin, L., Landais, A., Toyé Mahamadou Kele, H., Lemieux-Dudon, B., Parrenin, F., Martinerie, P., Blayo, E., Blunier, T., Capron, E., Chappellaz, J., Rasmussen, S.O., Severi, M., Svensson, A., Vinther,

B., Wolff, E.W., 2013. The Antarctic ice core chronology (AICC2012): An optimized multi-parameter and multi-site dating approach for the last 120 thousand years. Climate of the Past 9, 1733–1748.

Wenzens, G., 2005. Glacier advances east of the Southern Andes between the Last Glacial Maximum and 5,000 BP compared with lake terraces of the endorrheic Lago Cardiel (49 degrees S, Patagonia, Argentina). Zeitschrift Fur Geomorphologie 49, 433–454.

Zech, R., 2012. A late pleistocene glacial chronology from the Kitschi-Kurumdu Valley, Tien Shan (Kyrgyzstan), based on 10Be surface exposure dating. Quaternary Research 77, 281–288.

Zech, R., Zech, J., Kull, C., Kubik, P.W., Veit, H., 2011. Early last glacial maximum in the southern Central Andes reveals northward shift of the westerlies at ˜39 ka. Climate of the Past 7, 41–46.